

---

# Edge Inference with Fully Differentiable Quantized Mixed Precision Neural Networks

---

Clemens JS Schaefer<sup>\*†</sup>, Siddharth Joshi<sup>†</sup>, Shan Li<sup>‡</sup> and Raul Blazquez<sup>‡</sup>

<sup>†</sup> University of Notre Dame, Notre Dame, IN, USA

<sup>‡</sup> Google LLC, Mountain View, CA, USA

*{cschaefer, sjoshi2}@nd.edu, {lishanok, rblazquez}@google.com*

## Abstract

The large computing and memory cost of deep neural networks (DNNs) often precludes their use in resource-constrained devices. Quantizing the parameters and operations to lower bit-precision offers substantial memory and energy savings for neural network inference, facilitating the use of DNNs on edge computing platforms. Recent efforts at quantizing DNNs have employed a range of techniques encompassing progressive quantization, step-size adaptation, and gradient scaling. This paper proposes a new quantization approach for mixed precision convolutional neural networks (CNNs) targeting edge-computing. Our method establishes a new pareto frontier in model accuracy and memory footprint demonstrating a range of quantized models, delivering best-in-class accuracy below 4.3 MB of weights (wgts.) and activations (acts.). Our main contributions are: (i) hardware-aware heterogeneous differentiable quantization with tensor-sliced learned precision, (ii) targeted gradient modification for wgts. and acts. to mitigate quantization errors, and (iii) a multi-phase learning schedule to address instability in learning arising from updates to the learned quantizer and model parameters. We demonstrate the effectiveness of our techniques on the ImageNet dataset across a range of models including EfficientNet-Lite0 (e.g., 4.14MB of wgts. and acts. at 67.66% accuracy) and MobileNetV2 (e.g., 3.51MB wgts. and acts. at 65.39% accuracy).

## 1 Introduction

Deep neural networks (DNNs) demonstrate remarkable performance at computer vision tasks, notably being the defacto standard methods employed for large scale image recognition ([36, 4]). However, modern deep learning models require substantial compute and memory resources. This presents a challenge in deploying DNNs on resource constrained edge hardware.

Current efforts at reducing the energy and memory footprint of DNNs include the design of hardware-friendly DNN models, the development of low-power/latency hardware, model pruning, and quantizing DNNs to operate at lower precision[29, 27, 31]. Since low-precision operations can simultaneously lower the memory footprint, increase throughput, and lower the latency for DNN inference, DNN quantization has become increasingly important [20]. In particular, with recent DNN accelerators [35, 21] and graphics processing units (GPUs) [28] offering support for mixed-precision computing, these benefits can be realized on existing hardware [34]. Additionally, with the increasing prevalence of field programmable gate arrays (FPGAs) for deploying DNNs, an increasing number of platforms provide support for multiple-precision DNNs. However, quantized DNN models are unable to fully leverage such hardware capabilities. In particular, most model quantization systems focus on weight quantization, ignoring the high energy and latency cost due to moving and storing

---

<sup>\*</sup>Work partly conducted while interning at Google LLC

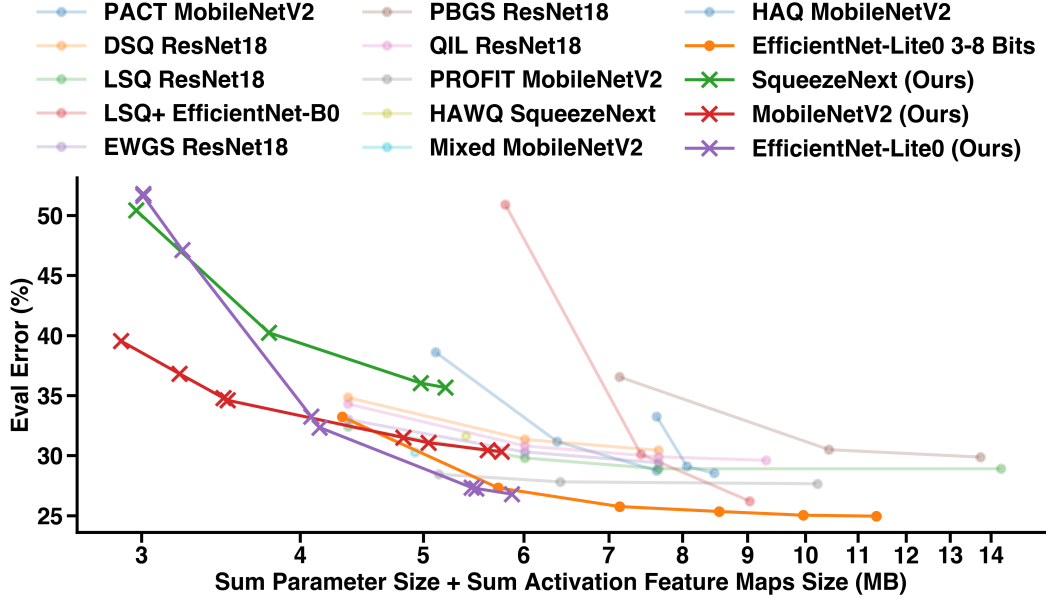


Figure 1: Our results quantizing different models compared to state-of-the-art. Network size (sum of parameters and activations) is compared to the evaluation error on the ImageNet dataset. Models quantized with our method occupy the pareto-frontier, delivering smaller multi-bit networks at higher accuracy. We shows results from: PACT[6], DSQ[13], LSQ[11], LSQ+[2], EWGS[24], PBGS[23], QIL[22], PROFIT[26], HAWQ[9], HAQ[32], Mixed[30]

activations. Benchmarking has shown that the activation energy from intermediate layers dominates in edge computing systems [5].

Previous research [34, 30, 32] has shown promising results with heterogeneous quantization, allocating memory resources per layer. This form of quantization can facilitate a wider range of trade offs between networks size and accuracy. Building on this insight, we focus this paper on developing compact DNN models extremely low memory footprints. We report best-in-class results for models with a total memory footprint below 4.3 MB.

In this paper we: (i) present a hardware-aware mixed precision differentiable quantization with per-tensor learned precision for activations and a fine-grained per-channel quantization for weights, (ii) propose a novel gradient modification scheme and provide comprehensive comparison against other gradient scaling techniques, and (iii) introduce a multi-phase learning-rate schedule to address instability in learning arising from updates to the learned quantizers. We show the effectiveness of our methods on the ImageNet dataset using the EfficientNet-Lite0, MobileNetV2, wide SqueezeNext, and ResNet18 architecture. We demonstrate state-of-the-art accuracy for multi bit-width models ranging from 2.89–4.3 MB total memory footprint. Across various architectures, our quantization scheme forms the pareto optimal frontier for model accuracy vs. model size.

## 2 Background

Uniform quantization is typically emulated in software by rounding and clipping floating point values, formalized as:

$$Q_u(x, d, q_{\max}) = \text{round} \left( \text{clip} \left( \frac{x}{d}, -q_{\max}, q_{\max} \right) \right) \cdot d. \quad (1)$$

Where  $Q_u$  is the quantization function,  $x$  the value to be quantized,  $d$  the step size and  $q_{\max}$  is the dynamic range. Achieving high model-accuracy given  $b$  bits to represent values, entails a careful choice of the dynamic range ( $q_{\max}$ ) and (implicitly) the step size ( $d$ ). The dynamic range relates to

the step size and the number of bits as  $b = \log(q_{\max}/d)$ . In this paper, we use *calibration* for the process of determining these values during training.

There are two main approaches to quantizing a floating point model: Post training quantization (PTQ) and Quantization Aware Training (QAT). PTQ does not typically require retraining or fine-tuning, with recent work by Dai et al. [7] demonstrating a 6 bit quantized ResNet-50 delivering 75.80% accuracy on ImageNet. However, the authors report limited success in but retaining accuracy in low-bit regimes, dropping from 75.80% with 6 bits to 7.11% with 3 bits. QAT takes into account quantization of weights and activations during training, and consequently has seen greater use in the low-bit regimes. However, QAT must address challenges arising from the non-differentiability of the quantization function which results in vanishing when propagated through multiple quantized layers.

## 2.1 Quantization Aware Training

The straight-through-estimator (STE) [1] is commonly used to avoid this problem, replacing the derivative of a discretizer (rounding) with that of an identity function. Essentially, ignoring the rounding function in the backward pass and preserving gradient flow.

To further enhance QAT performance, Choi et al. [6] introduce PACT which makes the dynamic range (see Eq. 1  $q_{\max}$ ) a trainable parameter. They achieve 75.3% evaluation accuracy on ImageNet with a ResNet50 quantized down to 3 bits while simultaneously stabilizing training. Jung et al. [22] examine the use of non-uniform quantization and study the effect of learned quantization levels. The resulting quantizer achieves 73.1% evaluation accuracy on ImageNet while using a ResNet34 quantized to 3 bits. However, non-uniform quantizers cannot always be mapped on to fixed-point arithmetic and can incur significant overhead when deployed or implemented in hardware [9]. Learning the step-size  $d$  while learning a uniform quantization scheme, Esser et al. [11] developed LSQ which achieves an accuracy of 74.3% on ImageNet using a 3-bit ResNet34. In LSQ+, Bhalgat et al. [2] build on this technique by parameterizing the symmetry of the quantizer to accommodate modern activation functions such as swish, h-swish and mish, which have limited, but critical negative excursions. They demonstrate the effectiveness of their method on modern architectures by achieving 69.9% accuracy with a 3-bit Efficient-B0 and 66.7% accuracy with a 3-bit MixNet on ImageNet. However, these methods do not quantize the first and last layers of the models, which typically incur significant performance degradation. In contrast, recent work using progressive-freezing and iterative training to quantize MobileNets [26] achieve 71.56% accuracy on ImageNet (note that MobileNets are significantly smaller than ResNets).

## 2.2 Heterogeneous Quantization

Model performance is not equally sensitive to quantization in different layers [26]. Prior work leverages this to allocate numerical precision on a per-layer basis [33, 26, 32, 10]. In HAQ [32], the authors use a reinforcement learning algorithm and a hardware simulator to generate energy and latency estimates used to optimize the bit-width of every layer. They report a  $1.9\times$  improvement to energy and latency while maintaining 8-bit levels of accuracy for MobileNet models. More recently, second order techniques like [9] use Hessian eigenvalues to determine quantization sensitivity and assign layer bit-widths. This Hessian aware trace-weighted quantization (HAWQ) offers 75.76% accuracy (ImageNet) for ResNet50 with an average of 2 bit weights and 4 bit activations.

Uhlich et al. [30] (label Mixed in Figure 1) formulate a fully differentiable quantization scheme, where both the step-size and the dynamic range are trainable, using a symmetric uniform quantizer  $Q_U(x, d, q_{\max})$ . This formulation implicitly learns the bit-width. Additionally, the authors add an additional constraint to the loss function to target a network weight size and maximum feature map size. Taken together, their improvements result in a MobileNetV2 with a weight memory footprint of 1.55 MB and a maximum activation feature size of 0.57MB, while delivering an accuracy of 69.74% on ImageNet (an estimated 4.93 MB for the wgt. and sum of act.).

## 2.3 Gradient Scaling for Quantization

Most models employ straight-through-estimators (STEs) in QAT for quantized neural networks essentially ignoring discretization in the backward pass. Alternatively some recently proposed techniques avoid this discrepancy by employing a smooth function, e.g., stacked tanh, prior to the

non-differentiable quantizer to emulate quantization effects facilitating gradient flow across layers (DSQ [13] in Figure 1). They demonstrate a 2-bit ResNet18 delivering 65.17% accuracy on ImageNet. Since the authors cascade this soft quantizer with a hard quantizer, they still employ an STE to propagate gradients in the backwards pass.

Kim et al. [23] (PBGs in Figure 1) propose gradient scaling as a regularizer to learn ‘easy to quantize’ networks. They recommend training models with gradients scaled to induce values that eventually fall on the quantization grids. The authors demonstrate results for a 4-b quantized ResNet18 trained to 63.45% evaluation accuracy on ImageNet. In the same vein, Nguyen et al. [25] achieve the same effect through regularization rather than direct modification of the gradients. They use the absolute cosine function for a 6-bit automatic speech recognition recurrent neural network with only a 2.68% accuracy degradation compared to the baseline model. Lee et al. [24] (EWGS in Figure 1) combine quantization in the forward pass and gradient scaling in the backward pass to account for discretization errors between inputs and outputs of the quantizer. They incorporate the sign and magnitude of the discretization error as well as second-order information to determine the gradient scaling factor. This method achieves 67% evaluation accuracy on ImageNet with ResNet18 quantized to 2 bits (a model with a total memory footprint of 4.36 MB including wghts. and sum of acts.).

### 3 Methods

Given a pretrained floating point model we quantize it in three phases: (i) homogeneous pre-training phase, (ii) a phase to learn precisions, and (iii) a final finetuning phase where only model parameters are updated (see Fig. 3). During all those phases we employ gradient scaling to account for discretization in the backward pass. We implement an initial calibration phase for both weights and activations using Gaussian calibration for the weights and the 99.99<sup>th</sup> percentile for the activations, which improves our homogeneous quantization performance by up to 1.22% for 3-bit EfficientNet compared to simple maximum calibration (see suppl. mat. Table 2 for details). During phase (ii) we employ penalty scheduling and reduce the frequency of quantizer parameter updates to combat learning instabilities. We also incorporate the weight and activation size penalty into the loss function like Uhlich et al. [30], resulting in:

$$L = CE(x, y) + \beta \max \left( \left( \sum_{l=1}^L b_l^w \cdot s_l^w \right) - t^w, 0 \right)^2 + \beta \max \left( \left( \sum_{l=1}^L b_l^a \cdot s_l^a \right) - t^a, 0 \right)^2. \quad (2)$$

Here,  $x$  is the input,  $y$  the target,  $CE$  stands for the cross entropy loss,  $b_l$  represents the bitwidth of layer  $l$ ,  $s_l$  is the number of parameters of a given layer and  $t$  is the target size for the model. The superscripts  $w$  and  $a$  indicate weights and activations respectively. We use rectified quadratic penalties to enable an accuracy vs. model size trade-off during training, with the rectification used to prevent penalization once the size budget is met. To prevent parameter explosion, we only use a single modulating factor  $\beta$  to control the penalty on model size.

#### 3.1 Quantization Training Dynamics

Learning both model parameters and bit-width allocations is necessarily a higher dimensional problem than just learning the parameters alone. This increases the search’s sensitivity to initial conditions. To mitigate this, we de-couple these two elements by starting out training on a homogeneously quantized network (from the pre-training) and then training the per-layer quantizer with progressively increasing pressure from the model size constraints. As shown in Figure 3 (left), the model suffers from dramatic accuracy degradation when the model size penalty is imposed. Often, this results in catastrophic training failure due to the model size penalty dominating cross-entropy loss. We use a soft-transition on the size penalty ( $\beta$ ) by linearly increasing  $\beta$  to its final value. This initial training can be viewed as enabling coarse navigation to the optimal in the solution space, followed by a more fine-grained descent towards the joint model-quantizer optima. As seen in Figure 3 (left), parameter updates can recover some lost accuracy after  $\beta$  saturates.

We observed model instability and training failure when both bit-precision and model parameters were updated frequently. Infrequent updates prevented thorough exploration of the model search space, resulting in models that were still similar to their homogeneously quantized initializations. We

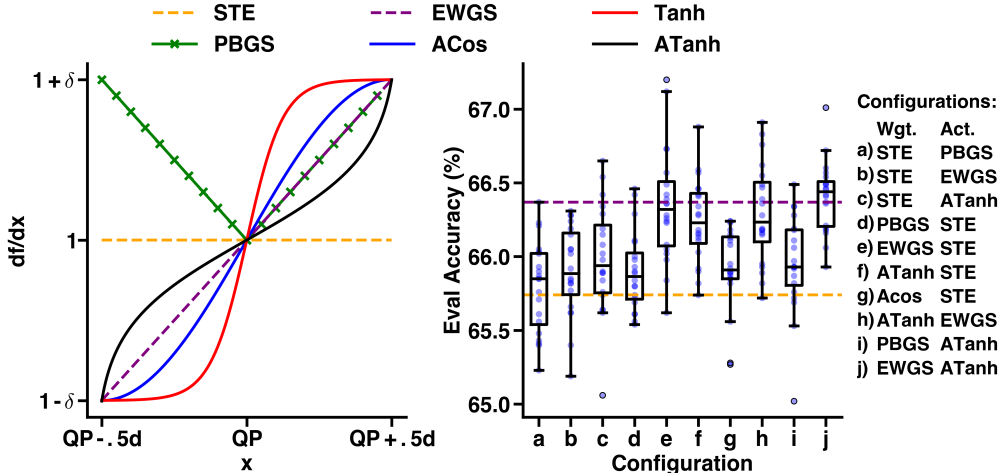


Figure 2: On the left we illustrate different gradient scaling functions: straight-through-estimators (STE [1]), elementwise gradient scaling (EWGS [24]), position based gradient scaling (PBGS [23]), absolute cosine regularization (Acos [25]) as well as hyperbolic tangent function (Tanh) and its inverse (InvTanh). Note that  $QP$  denotes quantization point,  $d$  is the step size and  $\delta$  is the magnitude control hyper parameter for gradient scaling. On the right we show the performance of mixed gradient scaling functions (e.g. different gradient scaling functions for weights and activations) on a homogeneous 3 bit EfficientNet-Lite0 on the ImageNet dataset.

addressed this by limiting the update frequency for the bit-precision parameters, restricting updates to every  $\Phi$  steps. In our experiments, an update frequency of  $\Phi = 20$  provided sufficient time for model statistics (e.g. batch norm) to stabilize and model parameters to adapt to the new precision level.

Subsequently, we enable finer-grained quantization by adapting the precision of the convolution weight kernels at a per-output-channel granularity (tensor slices). Most existing hardware with mixed-precision support can compute a single channel at a given precision. However, finer grained quantization can entail significant hardware overhead [19]. Indeed, the variation in dynamic range across channels from a heterogeneously quantized EfficientNet-Lite0 and MobileNetV2 demonstrate the efficiency gains available using this technique (See Figure 3 right). To prevent the gains from quantized operation getting negated, we ensure that quantization granularity is not too fine-grained. After these quantizer parameters converge, we freeze them by setting  $\beta = 0$  in eq. (2). This is followed by an additional fine-tuning period with a decaying learning rate to recover accuracy. In particular, our results suggest that batch normalization statistics are stabilized through this fine-tuning period, recovering accuracy.

### 3.2 Gradient Scaling

The STE operator is the de facto standard for enabling backpropagation through non-differentiable functions. We study how different gradient scaling techniques compare to STE across models and levels of precision. As shown in Figure 2, tanh-based gradient scaling for activations and linear scaling for weights [24] outperforms other combinations. We examine the effect of gradient scaling across multiple scaling functions ( $f(x)$ ) enumerated below (and shown in Figure 2 (left)):

1. Position based gradient scaling (PBGS) [23]:

$$\frac{\partial f}{\partial x} = 1 + \delta \cdot |x - \text{round}(x)|.$$

2. Element-wise gradient scaling (EWGS) [24]:

$$\frac{\partial f}{\partial x} = 1 + \delta \cdot \text{sign}(g_x) \cdot (x - \text{round}(x)).$$

3. Modified absolute cosine (ACos) [25]:

$$\frac{\partial f}{\partial x} = 1 + \delta \cdot \sin(\pi \cdot (x - \text{round}(x))).$$

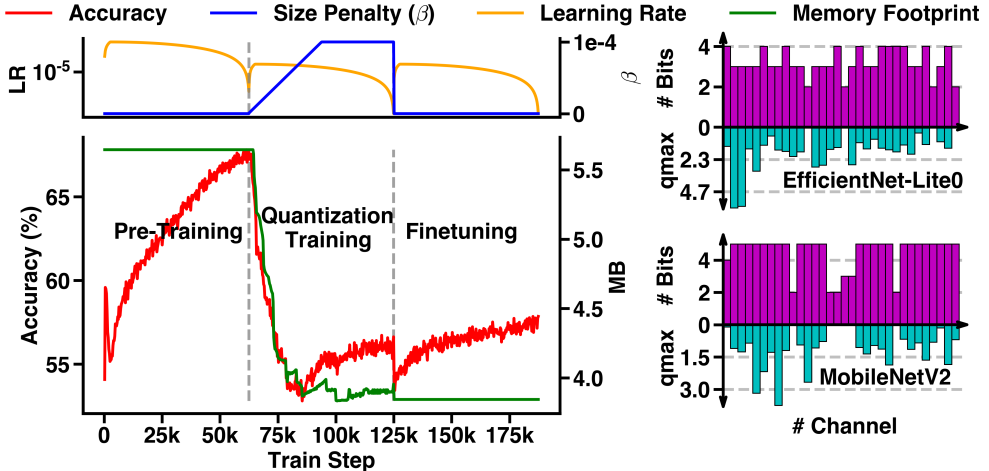


Figure 3: On the left illustrating the three phases of our mixed precision training method. The top left shows scheduled learning rate and size penalty ( $\beta$ ) term meanwhile the bottom left shows the evolution of model accuracy and model size. On the right we show an example per-channel bit allocation in a weight kernel of an EfficientNet-Lite0 and MobileNetV2. Extreme quantization is correlated to low dynamic range ( $q_{\max}$ ). However, the contra does not necessarily hold.

4. Generalized gradient scaling for hyperbolic tangent (Tanh):

$$\frac{\partial f}{\partial x} = 1 + \delta \cdot \text{sign}(g_x) \cdot \tanh(\alpha \cdot (x - \text{round}(x))).$$

5. Generalized gradient scaling for inverse hyperbolic tangent (InvTanh):

$$\frac{\partial f}{\partial x} = 1 + \delta \cdot \text{sign}(g_x) \cdot \text{arctanh}(\alpha \cdot (x - \text{round}(x))).$$

Here,  $\delta$  is a general hyperparameter to modulate the magnitude of gradient scaling and  $g_x$  is the gradient. We also introduce an additional hyperparameter,  $\alpha$ , to control the steepness of the hyperbolic tangent functions. Figure 2 (right) shows the performance of various gradient scaling techniques for activations and weights when homogeneously quantizing EfficientNet-Lite0 to 3 bits. We examined the effect over 20 trials and show the resulting distribution in Figure 2. The horizontal dotted lines represent the baseline performance (when both acts. and wgts. use the same scaling technique) of the STE and EWGS method respectively. We observe that different gradient scaling schemes benefit the training performance for weights and activations, owing in part to different underlying distributions. Indeed, employing STEs for both weights and activations provides the performance baseline. We note that the improvements derived from gradient scaling on activations only (configurations *a*, *b*, *c*) lead to lower performance gains when compared to applying gradient scaling on weights only (configurations *d*, *e*, *f*). This suggests that the performance gains from gradient scaling can be primarily attributed to gradient scaling of weights. Although configuration *e* (weights use EWGS and activations use STE) delivered the best single-run result, as seen in Figure 2, these results were not consistent across trials. Indeed, in some trials, this configuration performed worse than the baseline. Indeed, the majority of the performance gains from applying EWGS also observed in configuration *e*, where EWGS is only applied to weights while the activations use STEs. We observed that linear gradient scaling (EWGS) for weights and the inverse of the hyperbolic tangent scaling of activation gradients provides consistent improvement over the baseline, proving to be the more robust gradient-scaling technique. More comprehensive sensitivity analysis and analysis of computational overhead are provided in Figures 5 and 6 in the supplementary material.

## 4 Experiments

We demonstrate the effectiveness of our proposed recipe on the ImageNet [8] dataset across multiple models including EfficientNet-Lite0 [29], MobileNetv2 [27], wide SqueezeNext [12], and

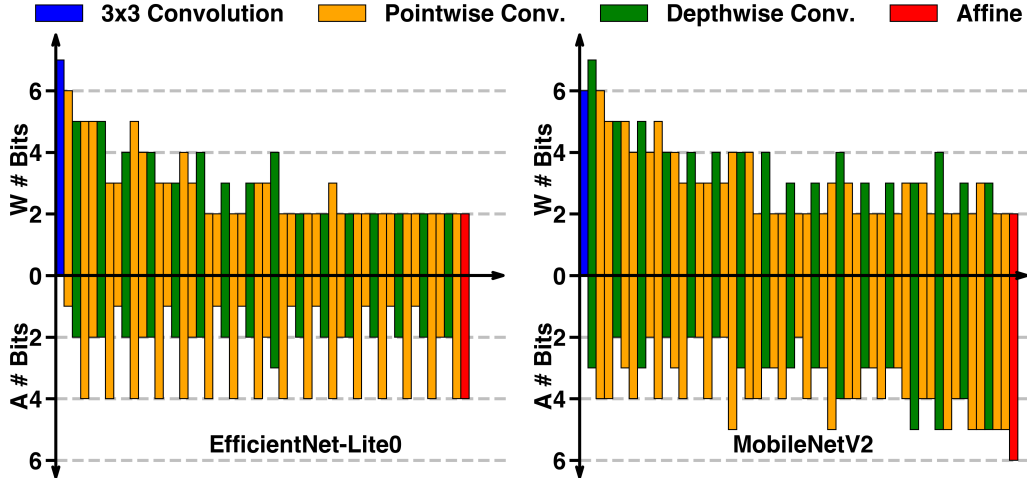


Figure 4: Internal bit allocation across layers of weights (up) and activations (down) for EfficientNet-Lite0 and MobileNetV2. Weights in the first layers have higher bit-widths for both models. Activations bitwidths for EfficientNet-Lite0 form a high precision path, e.g. activations which are residuals have higher precision. For both models the last affine layer has high precision.

ResNet18 [14]. We use the Flax [15] and Jax [3] frameworks to implement the networks, quantization scheme, and training routine. Our codes and configurations for experiments as well as model weights will be open sourced upon acceptance and, for now, they can be found in the supplementary materials. We ran our experiments on TPUv3 accelerators using the Google Cloud. Each experiment ran on a single instance which comprises 8 cores and 32GB memory.

We implement standard input pre-processing for training, randomly cropping images to  $224 \times 224$  with 3 channels (RGB), followed by input augmentation. Our augmentations include a random flip (left or right) and channel normalization (mean of 127 and standard deviation of 128). During evaluation the image is cropped around the center and no random flip is applied. Training uses the RMSProp optimizer [16] with 0.9 Nesterov momentum and a learning rate of  $10^{-4}$ . We increase the learning rate linearly from zero during the first two epochs and subsequently reduce it to zero in a cosine decay. Our training batch size is 1024, which is evenly split across the 8 cores of the TPU for single-program, multiple-data (SPMD) parallelism. We apply weight decay of  $10^{-5}$  and label smoothing with  $10^{-1}$  for improved accuracy. Each QAT training phase (pretraining, heterogenous training and finetuning) lasts 50 epochs.

Additionally, we set the gradient scale factor  $\delta$  ( $5 \cdot 10^{-3}$ ) through a small grid search. Results of the gradient scaling can be seen in Figure 2 (right) and for non-mixed configurations in supplementary materials Figure 5. Both show data from 20 trials on a 3-bit homogeneously quantized EfficientNet-Lite0, illustrating the variance in accuracy from employing gradient scaling methods. Figure 6 (supplementary materials) shows a smaller grid search for ideal gradient scaling on the same network quantized to 2 and 4 bits. Notably, variance in final accuracy increases when quantizing to fewer bits whereas the difference in accuracy gets exacerbated.

Figure 1 provides context for our results, comparing our techniques with state of the art quantization methods [6, 13, 11, 2, 24, 23, 22, 26, 9, 32, 30]. For references which did not report numbers for model size and sum of activation feature map size we compute the weight and activation sizes based on our replication of their work (all assumptions are shown in the supplementary materials table 4). The total network size (x axis in Fig. 1 includes batch norm parameters for which we assume a bfloat16 data type. Although no small-scale model (including our own) reports quantized batch normalization, Yao et al. [34] do report results from quantizing the batch norm layers for a 4 bit ResNet18 with a higher memory footprint than our reported results.

Our method improves the pareto frontier for model error and model size, with the greatest improvement seen in the sub 6 MB region. Here, we define size to be the sum of weights and sum of activation feature maps. We specifically optimize the total size of the activations, because of the high energy

Table 1: Effect of knowledge distillation (KD) on heterogeneously quantized networks and unquantized biases for the last affine layer. The first column shows the effect of KD on floating point networks the following columns are networks from the efficient frontier. Soft-label KD refers to a knowledge distillation technique where the target of the student network are the prediction of the teacher network [17]. Meanwhile penalty KD employs one-hot encoding as the target and adds a penalty term to force the student model prediction to align to the teacher model [26].

EfficientNet-Lite0								
Size (MB)	22.66	3.01	3.23	3.98	4.14	5.45	5.50	5.87
Base Accuracy (%)	75.53	48.37	52.87	66.46	67.66	72.56	72.75	73.21
Soft-Label KD	-0.31	0.21	0.24	0.11	0.10	0.17	0.10	-0.11
Penalty KD	-0.22	0.16	0.27	0.08	0.16	0.17	0.04	-0.11
No Bias Quant	-	1.56	1.16	0.20	0.26	0.14	0.15	0.00

MobileNetV2								
Size (MB)	20.25	2.89	3.21	3.48	3.51	4.82	5.05	5.62
Base Accuracy (%)	71.46	60.72	63.18	65.20	65.39	68.50	68.93	69.54
Soft-Label KD	0.15	0.36	0.12	0.13	0.23	0.12	-0.26	-0.24
Penalty KD	0.03	0.16	0.17	0.17	0.28	0.11	-0.19	-0.23
No Bias Quant	-	0.38	-0.01	0.24	0.08	0.21	0.05	0.16

cost arising from data movement for activations [5, 35]. To the best of our knowledge, we report best-in-class accuracy for multi-bit models in extreme constraint settings with less than 4.3 MB available for both weights and activations. Our efficient frontier (Figure 1) shows the degradation in performance across various target budgets and encapsulates the difference in robustness of various quantized model architectures. The EfficientNet-Lite0 architecture performs well for homogeneous quantization and heterogeneous quantizaton in a range between 4-6 MB total model size, meanwhile MobileNetV2 delivers better accuracy below 4 MB. We note the different scaling trends seen for quantized EfficientNet-Lite0 and MobileNetV2 , suggesting that MobileNetV2 may be more suitable for ultra-low budget applications. We included a wide SqueezeNext model due to its small weight footprint, however due to its depth the activation size dominate the overall model budget and making it a strictly worse model across the target budgets. For more ResNet18 and SqueezeNext results see A.3 in the supplementary materials.

Figure 4 shows the detailed layer-wise bit-allocation of heterogeneously quantized EfficientNet-Lite0 with a total size of 3.43 MB and MobileNetV2 with 3.41 MB. The EfficientNet-Lite0 architecture imposes greater precision in weights at the early layers of the network compared to the later layers. However the activations follow a constant pattern throughout the network. Notably, the activation of the last pointwise convolutional layer of a mobile inverted bottleneck (MBConv block) are higher in comparison to the other layers of MBConv blocks. Our results suggest that pointwise convolutional layers that have both residual and direct inputs require much higher precision to prevent quantization-induced information loss. This high precision bit-allocation indicates a critical information flow pathway. The MobileNetV2 bit allocation is similar to that of EfficientNet-Lite0, with higher precision weights in the initial layers which reduce with network depth. The critical path for the activation is not as pronounced as it is for the EfficientNet architecture and additionally high activation bit-width are allocated to layers closer to the final affine layer whose activation bit-width is the highest.

#### 4.1 Knowledge Distillation

Recently proposed quantization techniques have shown promising results by employing knowledge distillation (KD). We examine the impact of using KD for EfficientNet-Lite0 and MobileNetV2 occupying our pareto frontier. We use the KD process in [17], using soft labels created by a B16 vision transformer [4] with an accuracy of 85.49% (soft-label KD). We also examined the knowledge distillation technique employed by PROFIT [26], here the knowledge of the teacher model is induced into the student model through a penalty term in the loss function (penalty KD). The results summarized in Table 1 show that knowledge distillation can have a positive effect on the accuracy of

up to 0.36% but can also have negative effects. Neither of the KD techniques examined dramatically altered the model accuracy across the pareto frontier.

## 4.2 Bias Quantization

While our reported models quantize biases, we also report the effect of keeping biases at higher bfloat16 precision. Typically, accelerators can pre-load biases into the hardware accumulator, minimizing the energy impact. We summarize the impact of bias quantization in Table 1. Crucially, we note that MobileNetV2 at larger memory budgets do not see significant accuracy benefits ( $\leq 0.01\%$  higher accuracy in models of interest). However, EfficientNet-Lite0 models with tight memory budgets do see an increase their accuracy by approx. 1.56%.

## 5 Conclusions

We devise a training recipe for heterogeneously quantized neural networks where bit-widths are trained alongside model parameters and precision can be more flexibly allocated where needed. We enhance our training recipe with a novel gradient scaling technique to account for discretization due to quantization in the backward pass. Combined with careful penalty scheduling and alternating parameters updates as well as more fine-grained quantization we achieve a new state-of-the-art pareto optimal frontier of model size (including weights and activations) against performance (evaluation error) on the ImageNet dataset. Our method especially enables, to the best of our knowledge, best in class multi-bit neural networks which are smaller than 4.3 MB. Additionally we analyzed the bit allocation of the EfficientNet-Lite0 and MobileNetV2 architecture pointing out critical paths for activations and high bit-width requirements for weights in early layers of DNNs.

### 5.1 Limitations

The main limitation of our work is that to achieve a specific model size we use standard gradient descent optimization with penalties on the loss function which does not guarantee that the model size constraint will be fulfilled. The size constraints are part of the loss function and with a sufficiently large penalty factor ( $\beta$ ) the chance of fulfilling the constraint can substantially increase but simultaneously performance might be sacrificed. Furthermore, our method does not guarantee a solution on the efficient frontier. See Figures A.3 and A.3 in the supplementary materials where we summarize the sensitivity of different elements of our technique across multiple training runs. Typical solutions are within 1% or on the pareto frontier however some memory constraints prove especially hard to quantize efficiently on some networks, e.g. EfficientLite-0 around 5 MB yields sub-optimal solutions at two different accuracy levels both more than 1% away from the pareto frontier. Due to convergence limitations, we did not examine techniques for binarization and terenerization which could further improve the memory and energy footprint of these models.

Like related work, we do not quantize batch normalization parameters which contribute significantly to the model size post quantization. Techniques to “fold” these parameters into the convolution or affine layers have been proposed that could be leveraged to minimize this [20].

### 5.2 Societal Impact

Our work describes a general technique to train mixed precision neural networks and demonstrates its performance with image classification on the ImageNet dataset. In principle, our techniques can be applied to other domains as well. Our quantization method trades-off accuracy for model size. We have, however, not analyzed what the model forgets when its size constraints are tightened. Other research have recently investigated this issue for model compression [18]. Similar analysis for mixed precision quantization remains open. We foresee the primary impact to society being a reduction in the cost of deploying machine learning systems on edge devices, reducing the energy consumption and carbon footprint. However, widespread deployment of ML on such devices could see negative uses, e.g., surveillance. Additional negative impacts might arise due to the need for mixed-precision accelerators which might increase the barrier to entry for deploying such models.

## Acknowledgments

Research supported with Cloud TPUs from Google’s TPU Research Cloud (TRC)

## References

- [1] Yoshua Bengio, Nicholas Léonard, and Aaron Courville. Estimating or propagating gradients through stochastic neurons for conditional computation. *arXiv preprint arXiv:1308.3432*, 2013.
- [2] Yash Bhalgat, Jinwon Lee, Markus Nagel, Tijmen Blankevoort, and Nojun Kwak. Lsq+: Improving low-bit quantization through learnable offsets and better initialization. In *Proceedings of the IEEE/CVF Conference on Computer Vision and Pattern Recognition Workshops*, pages 696–697, 2020.
- [3] James Bradbury, Roy Frostig, Peter Hawkins, Matthew James Johnson, Chris Leary, Dougal Maclaurin, George Necula, Adam Paszke, Jake VanderPlas, Skye Wanderman-Milne, and Qiao Zhang. JAX: composable transformations of Python+NumPy programs, 2018. URL <http://github.com/google/jax>.
- [4] Xiangning Chen, Cho-Jui Hsieh, and Boqing Gong. When vision transformers outperform resnets without pre-training or strong data augmentations. *arXiv preprint arXiv:2106.01548*, 2021.
- [5] Yu-Hsin Chen, Tien-Ju Yang, Joel Emer, and Vivienne Sze. Eyeriss v2: A flexible accelerator for emerging deep neural networks on mobile devices. *IEEE Journal on Emerging and Selected Topics in Circuits and Systems*, 9(2):292–308, 2019.
- [6] Jungwook Choi, Zhuo Wang, Swagath Venkataramani, Pierce I-Jen Chuang, Vijayalakshmi Srinivasan, and Kailash Gopalakrishnan. Pact: Parameterized clipping activation for quantized neural networks. *arXiv preprint arXiv:1805.06085*, 2018.
- [7] Steve Dai, Rangha Venkatesan, Mark Ren, Brian Zimmer, William Dally, and Brucek Khailany. Vs-quant: Per-vector scaled quantization for accurate low-precision neural network inference. *Proceedings of Machine Learning and Systems*, 3:873–884, 2021.
- [8] Jia Deng, Wei Dong, Richard Socher, Li-Jia Li, Kai Li, and Li Fei-Fei. Imagenet: A large-scale hierarchical image database. In *2009 IEEE conference on computer vision and pattern recognition*, pages 248–255. Ieee, 2009.
- [9] Zhen Dong, Zhewei Yao, Daiyaan Arfeen, Amir Gholami, Michael W Mahoney, and Kurt Keutzer. Hawq-v2: Hessian aware trace-weighted quantization of neural networks. *Advances in neural information processing systems*, 33:18518–18529, 2020.
- [10] Ahmed T Elthakeb, Prannoy Pilligundla, Fatemeh Sadat Mireshghallah, Amir Yazdanbakhsh, and Hadi Esmaeilzadeh. Releq: A reinforcement learning approach for deep quantization of neural networks. *arXiv preprint arXiv:1811.01704*, 2018.
- [11] Steven K Esser, Jeffrey L McKinstry, Deepika Bablani, Rathinakumar Appuswamy, and Dharmendra S Modha. Learned step size quantization. *arXiv preprint arXiv:1902.08153*, 2019.
- [12] Amir Gholami, Kiseok Kwon, Bichen Wu, Zizheng Tai, Xiangyu Yue, Peter Jin, Sicheng Zhao, and Kurt Keutzer. SqueezeNext: Hardware-aware neural network design. In *Proceedings of the IEEE Conference on Computer Vision and Pattern Recognition Workshops*, pages 1638–1647, 2018.
- [13] Ruihao Gong, Xianglong Liu, Shenghu Jiang, Tianxiang Li, Peng Hu, Jiazen Lin, Fengwei Yu, and Junjie Yan. Differentiable soft quantization: Bridging full-precision and low-bit neural networks. In *Proceedings of the IEEE/CVF International Conference on Computer Vision*, pages 4852–4861, 2019.
- [14] Kaiming He, Xiangyu Zhang, Shaoqing Ren, and Jian Sun. Deep residual learning for image recognition. In *Proceedings of the IEEE conference on computer vision and pattern recognition*, pages 770–778, 2016.

[15] Jonathan Heek, Anselm Levskaya, Avital Oliver, Marvin Ritter, Bertrand Rondepierre, Andreas Steiner, and Marc van Zee. Flax: A neural network library and ecosystem for JAX, 2020. URL <http://github.com/google/flax>.

[16] Matteo Hessel, David Budden, Fabio Viola, Mihaela Rosca, Eren Sezener, and Tom Hennigan. Optax: composable gradient transformation and optimisation, in jax!, 2020. URL <http://github.com/deepmind/optax>.

[17] Geoffrey Hinton, Oriol Vinyals, Jeff Dean, et al. Distilling the knowledge in a neural network. *arXiv preprint arXiv:1503.02531*, 2(7), 2015.

[18] Sara Hooker, Aaron Courville, Gregory Clark, Yann Dauphin, and Andrea Frome. What do compressed deep neural networks forget? *arXiv preprint arXiv:1911.05248*, 2019.

[19] Ehab M Ibrahim, Linyan Mei, and Marian Verhelst. Survey and benchmarking of precision-scalable mac arrays for embedded dnn processing. *arXiv preprint arXiv:2108.04773*, 2021.

[20] Benoit Jacob, Skirmantas Kligys, Bo Chen, Menglong Zhu, Matthew Tang, Andrew Howard, Hartwig Adam, and Dmitry Kalenichenko. Quantization and training of neural networks for efficient integer-arithmetic-only inference. In *Proceedings of the IEEE conference on computer vision and pattern recognition*, pages 2704–2713, 2018.

[21] Norman P Jouppi, Cliff Young, Nishant Patil, David Patterson, Gaurav Agrawal, Raminder Bajwa, Sarah Bates, Suresh Bhatia, Nan Boden, Al Borchers, et al. In-datacenter performance analysis of a tensor processing unit. In *Proceedings of the 44th annual international symposium on computer architecture*, pages 1–12, 2017.

[22] Sangil Jung, Changyong Son, Seohyung Lee, Jinwoo Son, Jae-Joon Han, Youngjun Kwak, Sung Ju Hwang, and Changkyu Choi. Learning to quantize deep networks by optimizing quantization intervals with task loss. In *Proceedings of the IEEE/CVF Conference on Computer Vision and Pattern Recognition*, pages 4350–4359, 2019.

[23] Jangho Kim, KiYoon Yoo, and Nojun Kwak. Position-based scaled gradient for model quantization and pruning. *Advances in Neural Information Processing Systems*, 33:20415–20426, 2020.

[24] Junghyup Lee, Dohyung Kim, and Bumsup Ham. Network quantization with element-wise gradient scaling. In *Proceedings of the IEEE/CVF Conference on Computer Vision and Pattern Recognition*, pages 6448–6457, 2021.

[25] Hieu Duy Nguyen, Anastasios Alexandridis, and Athanasios Mouchtaris. Quantization aware training with absolute-cosine regularization for automatic speech recognition. In *Interspeech*, pages 3366–3370, 2020.

[26] Eunhyeok Park and Sungjoo Yoo. Profit: A novel training method for sub-4-bit mobilenet models. In *European Conference on Computer Vision*, pages 430–446. Springer, 2020.

[27] Mark Sandler, Andrew Howard, Menglong Zhu, Andrey Zhmoginov, and Liang-Chieh Chen. Mobilenetv2: Inverted residuals and linear bottlenecks. In *Proceedings of the IEEE conference on computer vision and pattern recognition*, pages 4510–4520, 2018.

[28] Mohammad Shoeybi, Mostafa Patwary, Raul Puri, Patrick LeGresley, Jared Casper, and Bryan Catanzaro. Megatron-LM: Training multi-billion parameter language models using model parallelism. *arXiv preprint arXiv:1909.08053*, 2019.

[29] Mingxing Tan and Quoc Le. Efficientnet: Rethinking model scaling for convolutional neural networks. In *International conference on machine learning*, pages 6105–6114. PMLR, 2019.

[30] Stefan Uhlich, Lukas Mauch, Fabien Cardinaux, Kazuki Yoshiyama, Javier Alonso Garcia, Stephen Tiedemann, Thomas Kemp, and Akira Nakamura. Mixed precision dnns: All you need is a good parametrization. *arXiv preprint arXiv:1905.11452*, 2019.

- [31] Weier Wan, Rajkumar Kubendran, Clemens Schaefer, S Burc Eryilmaz, Wenqiang Zhang, Dabin Wu, Stephen Deiss, Priyanka Raina, He Qian, Bin Gao, et al. Edge ai without compromise: Efficient, versatile and accurate neurocomputing in resistive random-access memory. *arXiv preprint arXiv:2108.07879*, 2021.
- [32] Kuan Wang, Zhijian Liu, Yujun Lin, Ji Lin, and Song Han. Haq: Hardware-aware automated quantization with mixed precision. In *Proceedings of the IEEE/CVF Conference on Computer Vision and Pattern Recognition*, pages 8612–8620, 2019.
- [33] Zhewei Yao, Amir Gholami, Kurt Keutzer, and Michael W Mahoney. Pyhessian: Neural networks through the lens of the hessian. In *2020 IEEE international conference on big data (Big data)*, pages 581–590. IEEE, 2020.
- [34] Zhewei Yao, Zhen Dong, Zhangcheng Zheng, Amir Gholami, Jiali Yu, Eric Tan, Leyuan Wang, Qijing Huang, Yida Wang, Michael Mahoney, et al. Hawq-v3: Dyadic neural network quantization. In *International Conference on Machine Learning*, pages 11875–11886. PMLR, 2021.
- [35] Amir Yazdanbakhsh, Kiran Seshadri, Berkin Akin, James Laudon, and Ravi Narayanaswami. An evaluation of edge tpu accelerators for convolutional neural networks. *arXiv preprint arXiv:2102.10423*, 2021.
- [36] Xiaohua Zhai, Alexander Kolesnikov, Neil Houlsby, and Lucas Beyer. Scaling vision transformers. *arXiv preprint arXiv:2106.04560*, 2021.

Table 2: Effect of different calibration methods on homogeneous bit-width training (3 bits) for a Efficient-Lite0 on the ImageNet dataset.

W/A	Max	$2 \times$ Mean	Gaussian	P99.9	P99.99	P99.999	P99.9999
Max	63.85%	63.78%	63.38%	63.24%	63.59%	63.73%	63.54%
$2 \times$ Mean	64.57%	0.10%	63.02%	64.51%	64.55%	64.72%	64.22%
Gaussian	64.72%	64.73%	64.90%	<b>65.07%</b>	64.75%	64.67%	64.79%
P99.9	64.67%	64.87%	64.64%	64.71%	64.64%	64.86%	64.88%
P99.99	64.56%	64.81%	64.44%	64.27%	64.45%	64.33%	64.51%
P99.999	64.29%	64.59%	64.50%	64.38%	63.96%	64.03%	64.25%
P99.9999	64.14%	64.23%	63.78%	63.73%	63.95%	64.34%	64.26%

Table 3: Effect of different calibration methods on homogeneous bit-width training (4 bits) for a Efficient-Lite0 on the ImageNet dataset.

W/A	Max	$2 \times$ Mean	Gaussian	P99.9	P99.99	P99.999	P99.9999
Max	72.08%	71.96%	71.89%	72.00%	71.87%	71.95%	72.08%
$2 \times$ Mean	72.25%	0.73%	72.09%	72.22%	72.15%	72.29%	72.30%
Gaussian	72.24%	72.27%	72.15%	72.26%	72.29%	72.29%	72.38%
P99.9	72.29%	72.44%	72.20%	72.31%	72.17%	72.12%	72.44%
P99.99	72.10%	72.10%	72.10%	72.32%	72.21%	72.27%	72.27%
P99.999	72.21%	72.11%	72.03%	71.95%	72.16%	72.25%	72.19%
P99.9999	72.09%	72.01%	72.10%	72.05%	71.97%	72.25%	72.02%

## A Supplementary Materials

We introduced our quantization method in Sections 2 and 3 of the main paper. Here, we will cover various sweeps, sensitivity analysis, and ablations that we have performed to more comprehensively study different quantization schemes.

### A.1 Calibration Methods

Model calibration refers to the process of determining a good step size ( $d$ ) and dynamic range ( $q_{\max}$ ) for the quantizer (see equation (1) for the definitions). Previous studies have shown that not only does the calibration method impact the final quantization outcome, the same method might not be optimal across different bitwidths [7]. Additionally, weights and activations have shown different sensitivities to quantization and dynamic range in computation, notably recent mixed precision work [9] seem to employ higher precision on activations. Consequently, we study how different calibration schemes might impact quantization performance through a coarse grid-search studying the quantization performance on a 3 bit homogeneous EfficientNet-Lite0 followed by quantization aware training for 50 epochs. Our results are summarized in Table 2, which show: (i) calibration method impact for weights vs. activations and (ii) calibration method impact at different bit precisions. The first phase of our training implements a homogeneously quantized model, with the dynamic range and step size being determined through the data of the first batch. We implement the following baselines to determine the clipping value ( $q_{\max}$ ): (i) the maximum value in the data, (ii)  $2 \times$  the mean of the data, (iii)  $\max(\mu + 3\sigma, |\mu - 3\sigma|)$  (Gaussian in table 2), and (iv) calibrating to the  $X^{\text{th}}$  percentile of the absolute value of the data over a range [7]. The choice of calibration scheme results in a 2.05% improvement over alternatives. The effect of different calibration schemes gets less pronounced at the higher precision (4 bits vs. 3 bits — see Table 3 for 4 bits).

### A.2 Comparison of Gradient Scaling Methods

In the main text we showed results for gradient scaling when using different gradient scaling methods for weights and activations, in Figure 5 we show the baseline results when the scaling methods are the same for weights and activations. The mean for STE and EWGS (best method in this experiment) also serve as orientations in Figure 2. We further show the effect of adding noise to the gradient instead of meaningful gradient scaling (Gaussian and uniform noise), surprisingly both methods

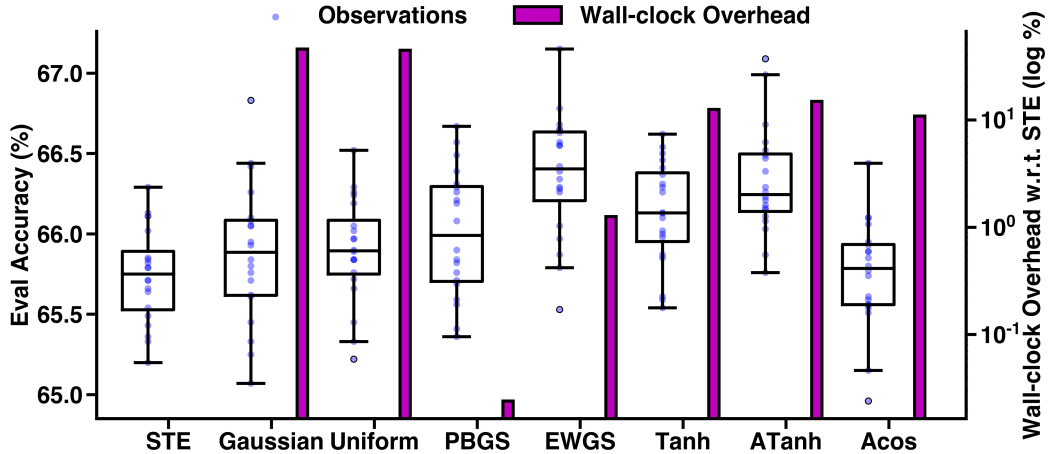


Figure 5: Comparison of gradient scaling methods on a EfficientNet-Lite0 with weights and activation both quantized to 3 bits with a gradient scale factor of 5e-3. STE ([1]) stands for the straight-through-estimator which does not modify the gradient meanwhile Gaussian and Uniform add random noise to the gradient in the backward pass. PBGS ([23]), EWGS ([24]) and Acos ([25]) scale the gradient based on the distance from the quantization point. We added two additional position based scaling methods Tanh and InvTanh. We also display the wall-clock time overhead of gradient scaling method in log percent compared to STE.

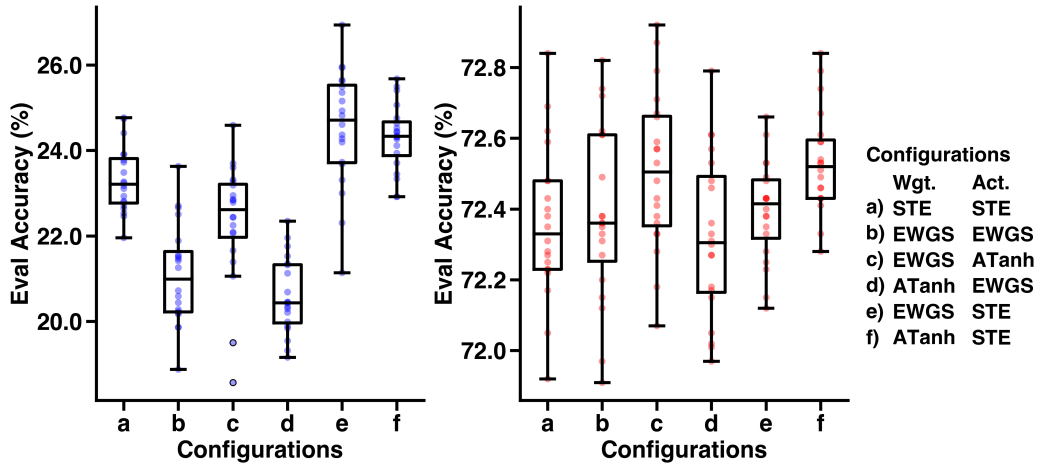


Figure 6: Comparison of selected gradient scaling methods on a homogeneously quantized 2 and 4 bit EfficientNet-Lite0 network. Accuracy numbers drop drastically for 2 bit networks and gradient scaling methods on activations show lower performance compared to the straight-through estimator method.

boost the accuracy beyond STE accuracy on average. Further we show the computational overhead measured in wall-clock time compare to the STE method, which does not perform any gradient modification. The methods which employ random noise are the most computationally expensive compared to the STE. Interestingly, PBGS only incurs minimal overheads while the others methods show substantial increase in compute time. Potentially, the sign operation on the gradient and the trigonometric operation seem to incur the most overhead.

We also analyzed the behaviour of several hand picked scaling methods on lower and higher bit widths comparable to what we have done in Figure 2. The results can be seen in Figure 6, showing that at 2 bits no method delivered better than 30% accuracy. The differences between these methods are less apparent ( $\leq 0.4\%$ ) at 4 bits.

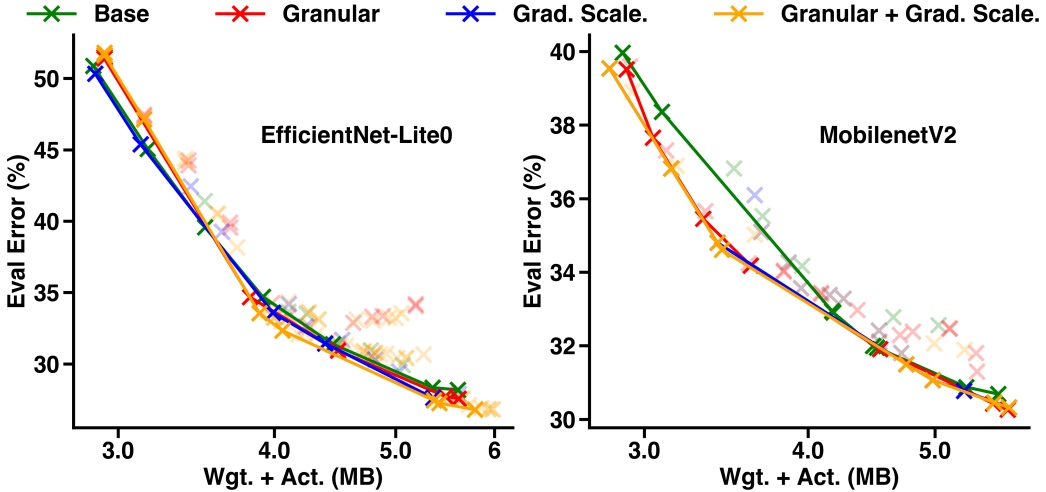


Figure 7: EfficientNet-Lite0 and MobileNetV2 mixed precision results showing all obtained data points, even those which are not pareto optimal.

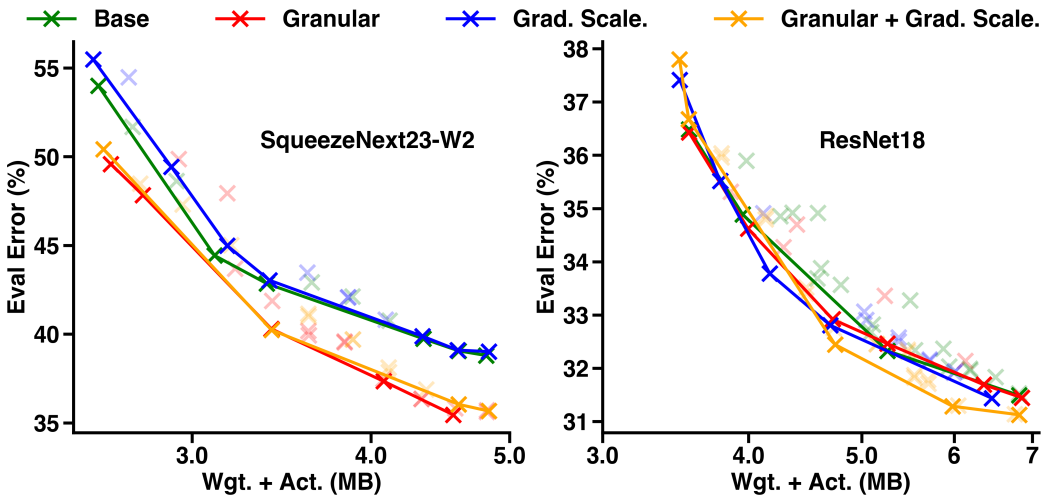


Figure 8: SqueezeNext23-W2 and ResNet18 mixed precision results showing all obtained data points, even those which are not pareto optimal.

### A.3 Effect of Granularity and Gradient Scaling

We demonstrate the effectiveness of our proposed quantization (see config. j in Figure 6), through ablation trials where we remove gradient scaling, fine-grained quantization, and their combination (base in Fig. 7 and 8). Across different models and target budgets, we see that our proposed fine-grained scheme consistently occupies the pareto, although not all trials perform as well (Figures 7 and 8).

### A.4 Assumption for Comparison to Other Work

To facilitate our comparisons in (Figure 1), we computed the memory footprint for weights and activations for different networks, assuming floating point (bf16) parameters for batch norm. If the references stated that they did not quantize the first and last layer ([6, 11, 2, 24, 22]), we assume they can use bfloat16 datatypes without any loss of accuracy. Table 4 states our assumptions about

Table 4: Numbers used to compute effective network sizes for other works.

	ResNet18	MobileNetV2	SqNxt23-W2	ENet-B0	ENet-Lite0
# Total Wgt.	11,689,512	3,504,872	20,670,016	5,288,548	4,652,008
# MVM Wgt.	11,679,912	3,470,760	20,485,184	5,246,532	4,609,992
# First Layer Wgt.	9,408	864	18,816	864	864
# Last Layer Wgt.	513,000	1,281,000	256,000	1,281,000	1,281,000
# BN Wgt.	9,600	34,112	184,832	42,016	42,016
# Total Sum Act.	2,032,640	6,678,112	3,962,208	8,982,784	6,676,256
# Last Layer Act.	512	1,280	256	1,280	1,280

networks sizes in terms of how many parameters models have in total, how many of those parameters are for matrix-vector multiplications, how many parameters are batch norm (BN) parameters and how many parameters belong to the first and last layers.